frontiers in Earth Science

ORIGINAL RESEARCH
published: 11 March 2022
doi: 10.3389/feart.2022.849167

Time Constraints of Late Cenozoic Tectonic Deformation of the Atushi Anticline, Southwestern Tian Shan: Evidence From Cosmogenic Nuclide Burial Age

Qingyu Chen[1,2], *Bihong Fu*[1]*, *Pilong Shi*[1] *and Ping Kong*[3]

[1]Aerospace Information Research Institute, Chinese Academy of Sciences, Beijing, China, [2]University of Chinese Academy of Sciences, Beijing, China, [3]Institute of Geology and Geophysics, Chinese Academy of Sciences, Beijing, China

With the latest uplift episode of Tian Shan occurring since early Miocene, a series of thrust–fold belts were formed in front of Tian Shan. The Kashi foreland thrust–fold belt (KFTB) provided a unique case to understand the ongoing intracontinental deformation within the Pamir–Tian Shan convergence zone (PTCZ). Previous cosmogenic nuclide chronological studies on growth folds suggested that the young thrust–fold belt in front of Pamir formed during 6–1.07 Ma. However, the age constraints of late Cenozoic deformation in front of southwestern Tian Shan are still debated. In this study, we attempt to constrain the initial deformation time of the NEE-striking Atushi anticline (ATA) in the KFTB through the cosmogenic nuclide burial dating data of growth strata near the boundary between Pliocene–Pleistocene Atushi Formation and Xiyu Formation (Xiyu Conglomerate), which are exposed in the southern limb of ATA. Moreover, detailed geological interpretations of multiple remote sensing images and field investigations are also carried out to document the late Cenozoic structural deformation and geomorphologic features of ATA. The $^{26}Al/^{10}Be$ burial dating data of four fine-grained samples reveal that the syntectonic deposit of ATA initiated at 1.79 ± 0.16 Ma, and the deposit of Xiyu Conglomerate started since 1.67 ± 0.18 Ma. Thus, we suggest that the thrust–folding of ATA began at ca.1.79 Ma and is currently still active.

Keywords: growth strata, Pliocene-Pleistocene sedimentary strata, $^{26}Al/^{10}Be$ burial age, tectonic deformation, Atushi anticline

OPEN ACCESS

Edited by:
Xuhua Shi,
Zhejiang University, China

Reviewed by:
Honghua Lu,
East China Normal University, China
Tao Li,
China Earthquake Administration, China

***Correspondence:**
Bihong Fu
fubh@aircas.ac.cn

Specialty section:
This article was submitted to Structural Geology and Tectonics, a section of the journal Frontiers in Earth Science

Received: *05 January 2022*
Accepted: *07 February 2022*
Published: *11 March 2022*

Citation:
Chen Q, Fu B, Shi P and Kong P (2022) Time Constraints of Late Cenozoic Tectonic Deformation of the Atushi Anticline, Southwestern Tian Shan: Evidence From Cosmogenic Nuclide Burial Age. Front. Earth Sci. 10:849167. doi: 10.3389/feart.2022.849167

INTRODUCTION

The Pamir–Tian Shan convergence zone (PTCZ) in western Tarim (**Figure 1A**) has resulted from the northward indentation of the India plate into the Eurasia plate since ~55 Ma (Molnar and Tapponnier, 1975; Burtman and Molnar, 1993). The ongoing India–Eurasia collision has caused a rejuvenation of Tian Shan orogen since early Miocene (Sobel and Dumitru, 1997; Yin et al., 1998; Sobel et al., 2006). After that, an accelerated uplift episode of Tian Shan and a rapid deformation of the Kashi foreland thrust–fold belt (KFTB) have generated 4 to 5 rows of thrust–fold belts in front of southwestern Tian Shan since Pliocene (Chen et al., 2002; Scharer et al., 2004; Heermance et al., 2008; Fu et al., 2010; Jia et al., 2015; Thompson-Jobe et al., 2018). The precisely constrained history of

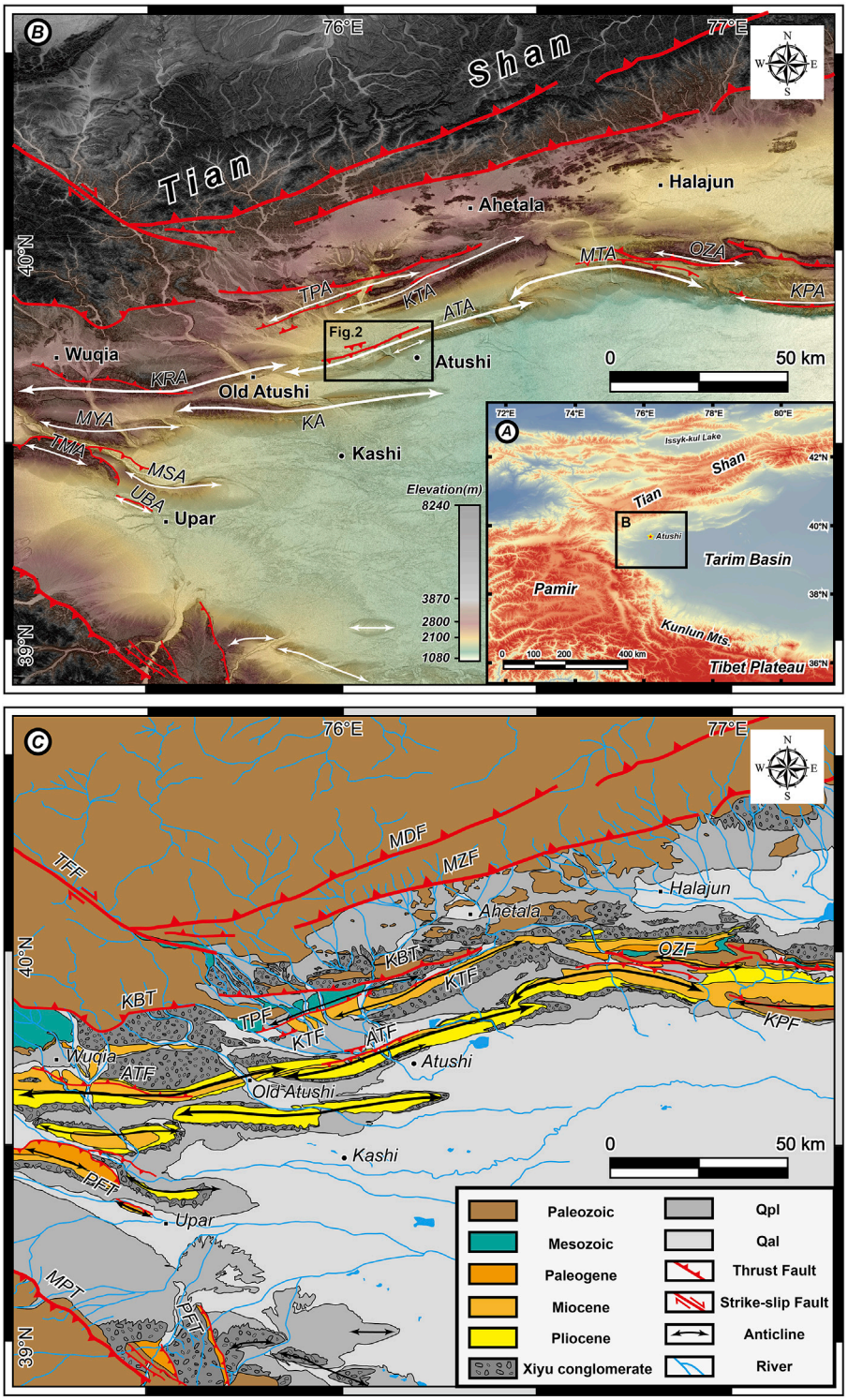

FIGURE 1 | Geological and geomorphological interpretation map of western Tarim. **(A)** Topographic features of Central Asia. The black polygon shows the location of the Pamir–Tian Shan convergence zone (PTCZ). The elevation data are from the 90-m SRTM DEM. **(B)** Major anticlines in PTCZ. The shaded relief map is based on the ALOS World 3D-30 m (AW3D30) **(C)** Geological interpretation map of PTCZ (based on our field investigation combined with interpretation of ASTER and Sentinel-2 multispectral images; Fu et al., 2010; Thompson-Jobe et al., 2018; Li et al., 2018). TPA, Tashipisake anticline; KTA, Keketamu Anticline; MTA, Mutule anticline; OZA, Ozr Goltau anticline; KPA, Kepingtage anticline; ATA, Atushi anticline; KRA, Kerato anticline; KA, Kashi anticline; MYA, Mingyaole anticline; TMA, Tumuan anticline; MSA, Mushi anticline; UBA, Ubulake anticline; TFF, Talas-Ferghana fault; MDF, Maidan fault; MZF, Muziduke fault; KBT, Kashi Basin thrust; TPF, Tashipisake fault; KTF, Keketamu fault; ATF, Atushi fault; OZF, Ozr Goltau fault; KPF, Kepingtage fault; PFT, Pamir frontal thrust; MPT, Main Pamir thrust.

tectonic deformation of thrust-related folds will provide a unique insight into the Cenozoic tectono-geomorphologic growth of PTCZ.

Syntectonic growth strata in foreland basins recorded the kinematic process of tectonic deformation. Since the early pioneer study of unique angular unconformity in the south of Pyrenees, Spain (Riba, 1976), the growth strata have been widely used to explore the coupling mechanisms between sedimentary basin and adjacent orogenic belt (Suppe et al., 1992; Shaw and Suppe, 1994; Chen et al., 2002; Heermance et al., 2008; Sun et al., 2009; Hardy and Cardozo 2021). Various age dating methods have been applied to document the basal age of growth strata, which could chronologically constrain the initiation of a fold growth (Chen et al., 2002; Sobel et al., 2006; Chen et al., 2007a; Heermance et al., 2008; Kong et al., 2011; Li et al., 2013; Thompson-Jobe et al., 2015).

Previous studies indicated that the growth strata are well developed around the thrust–fold belts in front of Pamir and Tian Shan (Chen et al., 2002; Scharer et al., 2004; Hubert-Ferrari et al., 2007; Sun and Zhang, 2009; Thompson-Jobe et al., 2018). In the recent studies (Thompson-Jobe et al., 2018; Thompson-Jobe et al., 2017), the $^{26}Al/^{10}Be$ dating data of Pliocene–Pleistocene growth strata and sedimentary units beneath the active faults developed along the Kerato anticline (KRA), Mingyaole anticline (MYA), Tumuan anticline (TMA), and Mushi anticline (MSA) in PTCZ have constrained the northward propagation of the northeastern Pamir thrust system since >5 Ma. However, the spatio-temporal process on the southward propagation of the KFTB in front of southwestern Tian Shan, particularly the initial deformation timing of the ATA, the southernmost thrust–fold belt in the KFTB, remains unclear (Chen et al., 2002; Heermance et al., 2007; Jia et al., 2015). It is difficult to date the thick coarse-grained Pliocene–Pleistocene sedimentary units, which are widely developed in the KFTB, with traditional chronological methods (Heermance et al., 2007; Balco and Shuster, 2009; Fu et al., 2010). Moreover, due to the tectonic uplift and long-term erosion in this region, the sedimentary facies frequently changed in the KFTB during the Neogene. Thus, the geological age of Pliocene–Pleistocene deposits in the KFTB is still controversial (Chen et al., 2002; Heermance et al., 2008).

The purpose of this study is to determine the initial deformation timing of ATA. To do this, we document in detail the late Cenozoic sedimentary units exposed at the ATA based on geological and geomorphological interpretations of the high-resolution multispectral satellite remote sensing images as well as the field investigations. Particularly, we meticulously recorded geometrical changes between the Pliocene–Pleistocene pre-growth strata and the growth strata along the cross-geological section in the western bank of Boguzi River by using unmanned aerial vehicle (UAV) horizontal imitating ground flight and field measurements. Finally, four fine-grained samples were collected from the Pliocene–Pleistocene sedimentary strata of the ATA to constrain the timing of late Cenozoic tectonic deformation of the anticline *via* $^{26}Al/^{10}Be$ burial age dating.

GEOLOGICAL SETTING

The KFTB is located in front of southwestern Tian Shan, where tectonic deformation and sedimentary response resulted from the interaction of Pamir, western Tarim, and southwestern Tian Shan (**Figure 1A**) (Allen et al., 1999; Avouac et al., 1993; Yin et al., 1998; Zhao et al., 2001; Scharer et al., 2004; Sobel et al., 2006; Fu et al., 2010; Gao et al., 2013). The KFTB is composed of a series of tight anticlines and broad synclines (**Figure 1B**) as well as the NE-NEE-striking thrust faults. Successively from north to south, they are Tashipisake Anticline (TPA), Keketamu anticline (KTA), Atushi anticline (ATA), and Kashi anticline (KA) (**Figure 1B**). The corresponding faults are Maidan fault (MDF), Muziduke fault (MZF), Kashi basin thrust fault (KBT), Tashipisake fault (TPF), Keketamu fault (KTF), and Atushi fault (ATF) (**Figure 1C**). MDF, MZF, KBT, and TPF dip to the north, which are exposed on the south flank of the anticlines. The south-dipping ATF and KTF are exposed on the north flank of the anticlines (Wu et al., 2019; Zhao et al., 2001; Chen et al., 2002; Scharer et al., 2004; Sobel et al., 2006; Heermance et al., 2007; Heermance et al., 2008; Fu et al., 2010; Jia et al., 2015; Li et al., 2018).

Affected by the southward expansion of southwestern Tian Shan, the sedimentary strata exposed on the surface are diverse and complex (**Figure 1C**). The Paleozoic strata exposed at the hanging wall of KBT are composed of Carboniferous limestone, shale, and Permian sandstone. The Mesozoic strata consist of Cretaceous thick red and orange sandstone interbedded with grayish-green siltstone (Chen et al., 2001; Scharer et al., 2004; Heermance et al., 2007). The Cenozoic strata mainly consist of the Miocene Pakabulake Formation (Pakabulake Formation), Pliocene Atushi Formation, and Xiyu Conglomerate (Chen et al., 2001; Heermance et al., 2007). The Pakabulake Formation is composed of brownish-red sandstone, siltstone, and gypsum at the upper layer (Fu et al., 2010). The Atushi Formation consists of grayish-yellow sandstone interbedded with thin brownish-red siltstone and mudstone. The Xiyu Formation is known as the Xiyu Conglomerate, distributed widely in the piedmonts of active orogenic belts in Xinjiang (Liu et al., 1996; Chen et al., 2001; Sun et al., 2004; Chen et al., 2007a; Sun et al., 2009; Sun and Zhang, 2009; Thompson-Jobe et al., 2018). The lithology and sedimentary facies of Xiyu Conglomerate are significantly different from its underlying strata. It is dark gray, gray massive conglomerate with grayish-yellow sandstone, siltstone layers or lens, main laminar flow, braided channel accumulation, and mostly alluvial–diluvial facies (Chen et al., 2000; Chen et al., 2007b).

Low-temperature thermochronological studies suggested that rapid topographical growth on the hanging wall of MDF and MZF could be constrained in 25–20 Ma. Afterwards, the structural stress delivered to KBT at 18–15 Ma (Sobel et al., 2006; Jia et al., 2015). The initial deformation age of TPA is constrained to 15–13.5 Ma according to sedimentary facies change, crosscutting relationships, and sedimentation rate (Heermance et al., 2008) as well as the detrital zircon age (Jia et al., 2015). The initial deforming age of KTA was defined at ~4 Ma that originated from the dating age of the growth strata and the sedimentation rate (Heermance et al., 2008).

At the southernmost part of KFTB, about 20-km-wide ATA and KA are developed themselves as shown in **Figure 1B** (Chen et al., 2001; Chen et al., 2002; Sobel et al., 2006; Tian et al., 2006; Yang et al., 2009; Li et al., 2018). Concerning the spatial distribution of ATA, some studies suggested that ATA is a reversed-S-shaped anticline, extending to near Wuqia county in the west and interacting with Mutule anticline (MTA) in the east (Scharer et al., 2004; Thompsom-Jobe et al., 2018). However, other researches considered that ATA is terminated at the Old Atushi town, and the western part belongs to the KRA (Heermance et al., 2008; Fu et al., 2010). Numerous studies have documented the Pliocene–Pleistocene strata exposed in ATA (Chen et al., 2002; Scharer et al., 2004; Sobel et al., 2006; Heermance et al., 2007; Heermance et al., 2008; Fu et al., 2010; Zhang et al., 2013; Jia et al., 2015; Thompson-Jobe et al., 2018). The NEE-SWW-striking ATF, a south-dipping thrust fault located at the northern flank of the ATA, is basically paralleled to the axis of ATA (**Figure 1B**). The age constraints from the magnetostratigraphy proposed that the northeastward lateral propagation and the growth of the ATA initiated at ~1.4 and ~1.2 Ma, respectively, in the eastern bank of Boguzi River and Ganhangou sections (Chen et al., 2002). Six pedestal terraces (including flood plain as T_0) are developed along the Boguzi River. All terraces are pedestal terraces, and the consolidated bed rock consisted of Pliocene mudstone, sandstone, and Lower Pleistocene conglomerate. The sediments of the terraces are mainly comprised of dark gray gravel and interbedded with a grayish-yellow sand layer containing sandy clay lenses. The diameter of the gravel is generally 2–10 cm, and the diameter of the individual large boulder is 20–30 cm. It is well rounded, and the main component is metamorphic sandstone. The deformation of the six terraces revealed that the ATA has experienced multi-stage uplifting and folding during the late Pleistocene (Yang et al., 2009). The youngest KA in the southernmost part of KFTB, a doubly plunging detachment fold with a steep northern limb and a gentle southern limb, extended over 60-km long (Chen et al., 2007a; Li et al., 2018; Li et al., 2019). The magnetostratigraphic data from two geologic sections at the south and north flanks of KA indicate that the anticline began growing at ~1.4 and ~1.07 Ma, respectively (Chen et al., 2007a).

DATA AND METHODS

Multiple Remote Sensing Data

Multispectral satellite remote sensing images are very useful to interpret the structural features and sedimentary units in the Pamir–Tian Shan convergence zone with an arid and semi-arid climate condition (Fu et al., 2010). Moreover, the duplication and the absence of strata and weathering make it difficult to identify the spatial distribution of stratigraphic units in the field (Heermance et al., 2007). In this study, multiple sources of satellite remote sensing data were used, which include the ASTER Visible and Near Infrared (VNIR, 15-m ground resolution) and short-wave infrared data (30-m ground resolution) and Sentinel-2 VNIR data (10-m ground resolution). For multispectral remote sensing data, an appropriate band selection of remote sensing data plays a key role in image enhancement, which is useful for geological interpretation and lithological extraction (**Figure 2A**). The ASTER false-color composite image (R: band ratio 2/1, G: band 3, and B: band ratio 5/8, **Figure 2A**) was able to distinguish different lithological units in this region. We also imposed ASTER multispectral image on the DEM data from ALOS World 3D-30 m (AW3D30) to generate 3D perspective images of a typical area (**Figure 4A**), which is beneficial for the geomorphologic feature analysis of KFTB.

Cosmogenic Nuclide Burial Dating

Cosmogenic nuclide burial dating, first proposed by Lal and Arnold (1985), relies on various decay constants for ^{10}Be and ^{26}Al (Granger and Muzikar, 2001). The assumption behind the method is that quartz is exposed to the cosmic rays at the Earth's surface for a period of time, acquiring certain amounts of ^{10}Be and ^{26}Al, respectively. When quartz is buried at a sufficient depth, the production of cosmogenic nuclides ceases, and decay becomes the dominant process affecting the concentrations of ^{10}Be and ^{26}Al (Granger and Muzikar, 2001; Granger et al., 2013). Cosmogenic nuclide burial data were widely used in interpreting exposed and the burial history of sediments or terrace surfaces (Balco and Shuster, 2009; Jungers and Heimsath, 2016) and dating the age of Late Cenozoic conglomerates (Kong et al., 2011; Thompson-Jobe et al., 2018). Compared with other means, cosmogenic nuclide dating is a direct way to measure samples without relying on existing symbolic age (like fossils and volcanic ash), which provided the numerical age of the samples instead of the correlated age or relative age (McCalpin and Nelson, 1996). ^{26}Al/^{10}Be burial dating is an advantage for dating Pliocene–Pleistocene clastic sediments that are challenging to be dated by other methods (Balco and Shuster, 2009; Thompson-Jobe et al., 2018). So far, we have selected ^{26}Al/^{10}Be burial dating method to constrain the geological age of Pliocene–Pleistocene conglomerates, which are exposed along the southern flank of ATA. Four samples were collected from the boundary between Atushi Formation and Xiyu Conglomerate (**Table 1**; **Figure 5B**). The sample preparations were processed at the cosmogenic nuclide laboratory of the Institute of Geology and Geophysics, Chinese Academy of Sciences in Beijing. The oxides were mixed with niobium and silver metal powders, and both ^{10}Be and ^{26}Al concentrations were measured by AMS at PRIME Lab at Purdue University. The concentrations of ^{10}Be/^{9}Be were normalized to the NIST standard SRM4325. Half-lives of 1.39 Ma (Korschinek et al., 2010) and 0.71 Ma and high-latitude, sea-level production rates of 4.6 and 31.1 atoms/g/year were used for ^{10}Be and ^{26}Al in the age calculation, respectively.

RESULTS

Geological and Geomorphological Interpretation of ATA

Based on the geological and geomorphological interpretation of satellite images and field investigations, our work depicted the geomorphologic expression and stratigraphic units of ATA in detail (**Figure 1**).

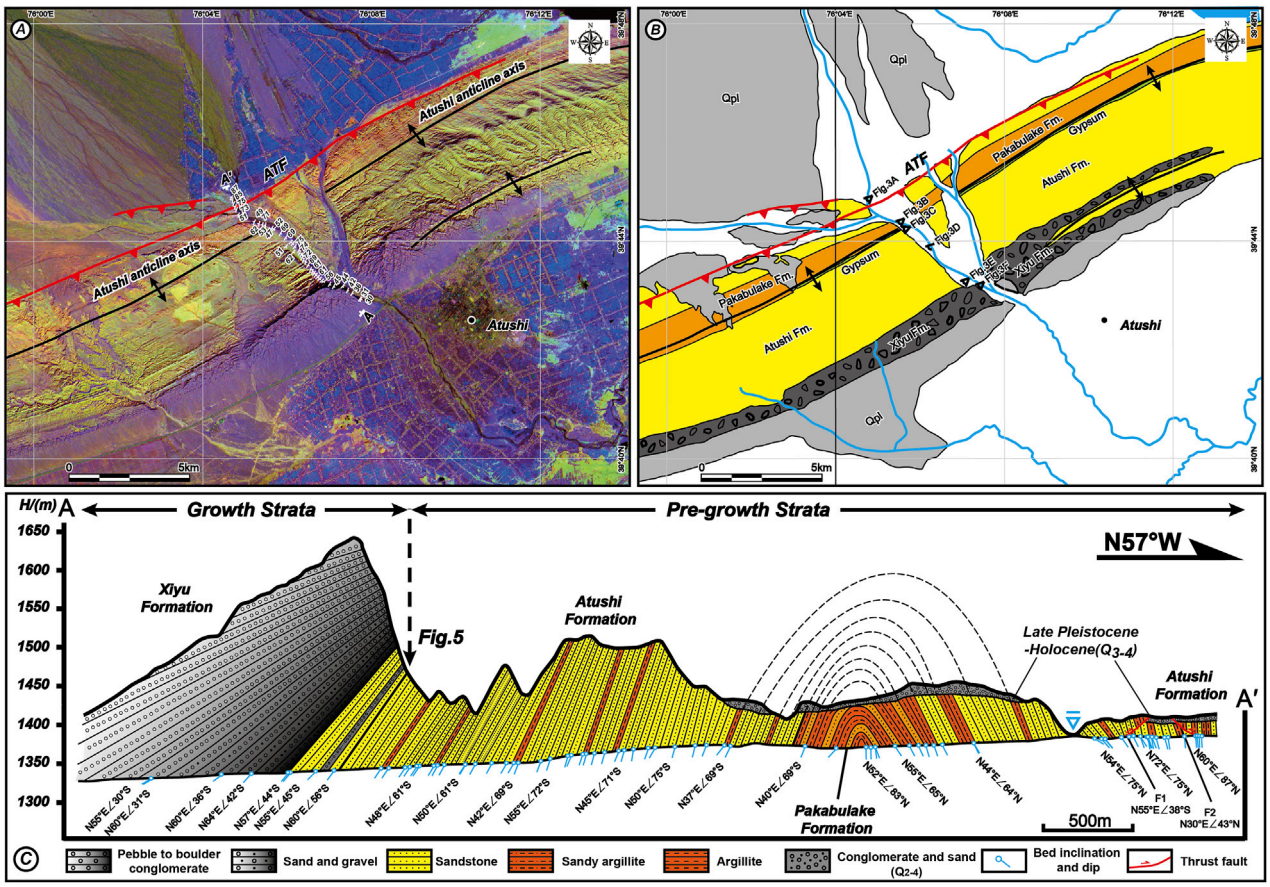

FIGURE 2 | (A) False-color ASTER composite image of 2/1(R), 3(G), and 5/8(B) of Atushi anticline. **(B)** Interpretation of satellite image. **(C)** Geological section observed on the western bank of Boguzi River (section A–A′ in **Figure 2A**).

TABLE 1 | Burial age of the upper layer of Atushi Formation and the lower layer of Xiyu Conglomerate.

Sample	Latitude (north)	Longitude (east)	Elevation (m)	Burial depth (m)	^{10}Be concentration ($\times10^4$ atg^{-1})	^{26}Al concentration ($\times10^4$ atg^{-1})	^{26}Al/^{10}Be	Burial age (Ma)
XY01	39°43.262′	76°06.856′	1,369	40	3.47 ± 0.13	9.2 ± 1.3	2.64 ± 0.38	1.94 ± 0.27
XY02	39°43.266′	76°06.845′	1,371	40	3.26 ± 0.15	8.4 ± 0.8	2.58 ± 0.27	1.99 ± 0.19
XY03	39°43.219′	76°06.897′	1,375	40	3.77 ± 0.16	10.7 ± 0.9	2.84 ± 0.26	1.79 ± 0.16
XY04	39°43.190′	76°06.940′	1,375	40	4.53 ± 0.16	13.7 ± 1.3	3.02 ± 0.30	1.67 ± 0.18

ATA is a growing fold with two asymmetric limbs (steep and narrow in the northern limb and gentle in the southern limb) and a tight hinge zone, with an axial surface dip to the south (**Figure 2C**). The surface expression of ATA extends to the Old Atushi town in the west and is interacted with MTA in the east, exceeding about 60 km along the axis of the fold (**Figure 1C**). A water gap formed in the middle part of ATA by the erosion of Boguzi River, and it provides an excellent geological section to observe and document the structural deformation and sedimentary features of ATA (**Figure 2**). Notably, our results indicated that a tight anticline developed at the east bank of Boguzi River along the southern flank of ATA (**Figure 2**).

The ATA has deformed Miocene Pakabulake Formation to Xiyu Conglomerate stratigraphic units (**Figure 2**). As shown in the ASTER false-color composite image (**Figure 2A**), the color patterns of Pakabulake Formation, Atushi Formation, and Xiyu Conglomerate are displayed as brownish-red, yellowish-green, and purplish-gray, respectively. The field investigations show that the Pakabulake Formation, exposed in the core of the anticline, is consisting of brownish-red argillite, sandy argillite, siltstone, and gypsum (**Figures**

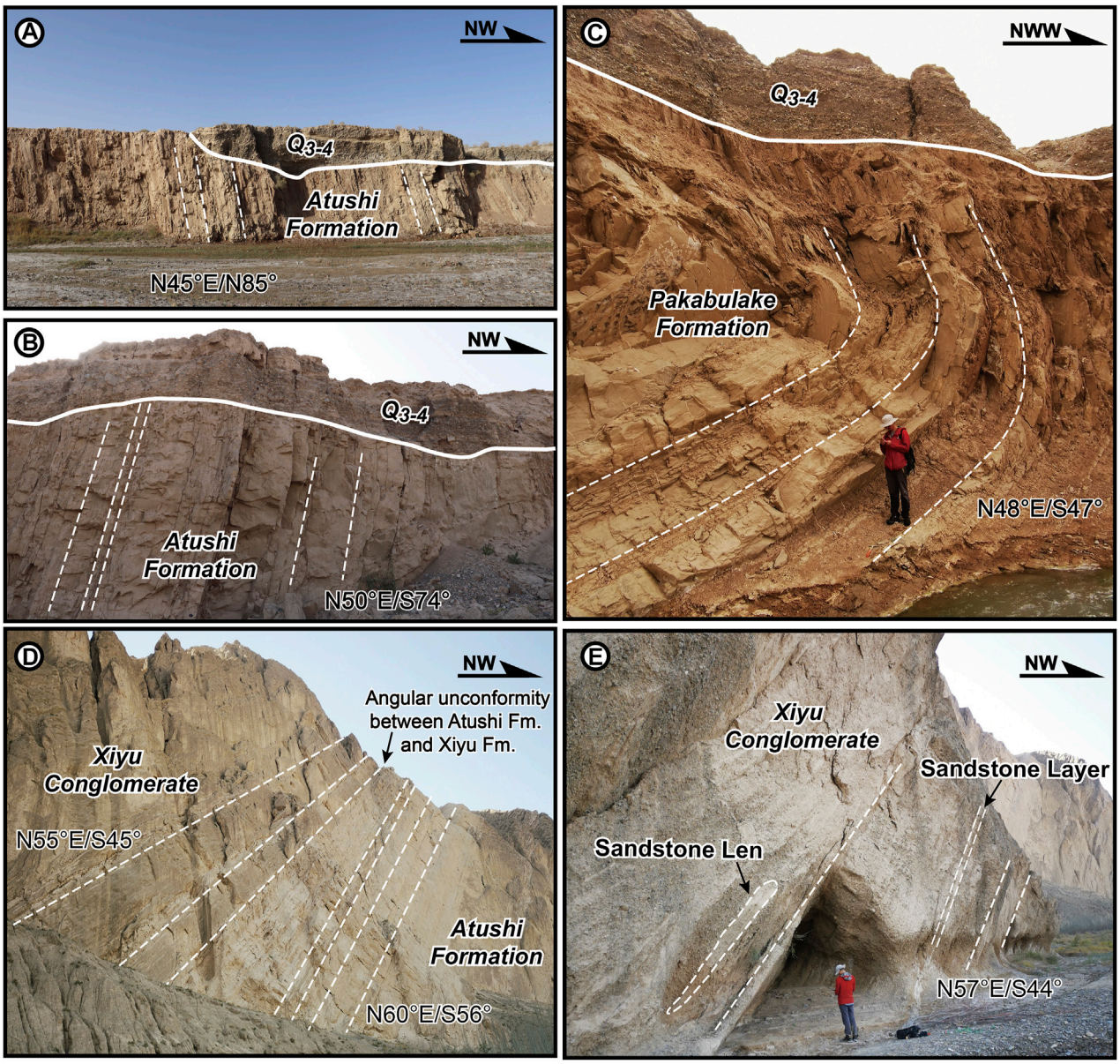

FIGURE 3 | Field photographs of the folded strata. **(A)** Picture of north-dipping Atushi Formation at the northern limb. **(B)** Picture of south-dipping Atushi Formation at the southern limb. **(C)** Intensive deformation of Pakabulake Formation in the core. **(D)** Angular unconformity between Atushi Formation and Xiyu Conglomerate. **(E)** Sandstone len and layer in gray Xiyu Conglomerate.

2B,C). The Atushi Formation is mainly composed of thick pale grayish-yellow sandstone, interbedded with thin brownish-red mudstone and containing a dark gray conglomerate at its top layer. The Xiyu Conglomerate is composed of a massive gray conglomerate containing grayish-yellow thin-bedded sandstone, siltstone layers, or lens (**Figure 3E**). The contact between Atushi Formation and Xiyu Conglomerate is displayed as a low-angular unconformity (**Figure 3D**).

The ATF is a south-dipping thrust fault extending along the north flank of ATA, which is affected by a northward thrusting deformation (**Figure 1B**; Yang et al., 2009; Fu et al., 2010). The fault scarps are developed on Late Quaternary proluvial and alluvial deposits of the Boguzi River along the ATF, showing that ATA is currently still active (**Figures 2B,C**).

$^{26}Al/^{10}Be$ Burial Age

Four fine-grained sandstone and siltstone samples were collected from the upper layer of Atushi Formation to the lower layer of the Xiyu Conglomerate at the southern flank of ATA (XY-01 to XY-04, **Figures 5B,C**). The sedimentary features of the upper layer of Atushi Formation and Xiyu Conglomerate are quite different. The upper layer of Atushi Formation is characterized by grayish

yellow sandstone interbedded with gray conglomerate, which is consisting of small-sized pebbles (1–3 cm) with fair sorting and subrounded psephicity. The Xiyu Formation is composed of dark gray, gray massive conglomerate, containing grayish-yellow thin-bedded sandstone, and siltstone layers or lens. The Xiyu Conglomerate is consisting of large- to medium-sized pebbles (5–10 cm) with bad sorting and subangular psephicity (**Figures 5D,E**). XY-01 and XY-02 were collected from the grayish-yellow sandstone and siltstone layers. XY-03 was sampled from the sandstone layer interbedded with conglomerate, where a low-angular unconformity has developed. These three samples were collected from the upper layer of Atushi Formation. XY-04 was sampled from the lenticular sandstone layer of Xiyu Conglomerate, near the boundary between the Atushi and Xiyu formations. To minimize production during incision and exhumation after the initial deposition, we collected samples from the sites that were well shielded by at least 30 m of rock. Sample information and ^{10}Be and ^{26}Al concentrations together with data on burial ages are shown in **Table 1**.

The ^{26}Al/^{10}Be ratios of XY-01, XY-02, XY-03, and XY-04, are 2.64 ± 0.38, 2.58 ± 0.27, 2.84 ± 0.26, and 3.02 ± 0.30, respectively. Although the ^{26}Al/^{10}Be ratio has a statistical difference from the model ^{26}Al/^{10}Be ratio of 6.76 ± 0.88 at the Earth's surface, the ^{26}Al/^{10}Be values of the four buried samples are consistent with each other. For buried samples that are within the range of muon production, the ^{10}Be and ^{26}Al concentrations will be functions of the initial concentrations at the time of burial, the burial time, and the burial depth as a function of time. Using the ^{26}Al/^{10}Be ratios, the burial ages range from 1.94 to 1.67 Ma. Our burial ages are almost equal to 1.7 Ma as obtained from the Boguzi River stratigraphic section (Sobel et al., 2006), but these are different from ~1.9 Ma for Xiyu Conglomerate as obtained by Chen et al. (2002) using magnetostratigraphy.

DISCUSSION

Geometries of the Growth Strata of ATA

Previous studies constrained the initial timing of deformation by dating the geologic age of the growth strata but rarely paid attention to the relationship between the growth mechanism of the fold and the sedimentary features of the growth strata (Sobel et al., 2006; Sun et al., 2009; Sun and Zhang, 2009). From the perspective of structural analysis, the growth mechanism of the thrust-related fold is mainly divided into two categories: hinge migration and hinge rotation (Shaw and Suppe, 1994; John and David, 1997; Hubert-Ferrari et al., 2007; Li et al., 2015; Li et al., 2018). Among the folds deformed by hinge migration, the geological age of the growth strata cannot simply represent the initial deformation timing of the fold. In this case, the hinge widening and dip angle might change over the hinge area in the pre-growth strata (Suppe et al., 1992; Salvini and Storti, 2002). On the other hand, the growth of the hinge rotation fold is through limb rotation, with the constant limb length and variable limb dip angle. The measurement of the onset age of the growth strata enabled us to constrain the initial deforming age of the limb rotation fold (Poblet et al., 1997).

Previous studies have already suggested that ATA belongs to the fold of the limb rotation growth mechanism based on the analyses of the geometry and dip panel (Chen et al., 2002), interpretation of seismic profile (Qu et al., 2001; Gao et al., 2013), and the measurement of the fold scarps (Li et al., 2018). According to our field investigation and mapping, we confirmed that the growth mechanism of ATA belongs to limb rotation (**Figure 4C**). The initial deposition of the growth strata could represent the beginning of the tectonic deformation of ATA.

Our results also show that the deformed late Cenozoic strata of Miocene Pakabulake Formation, Pliocene Atushi Formation, and Xiyu Conglomerate developed from the core to the southern limb of ATA (**Figure 2C**). Particularly, we carefully document the subtle change of bed dipping angles, bed width, and sedimentary features around the boundary of the growth and the pre-growth strata. Based on these criteria, we identified the sign layer that can represent the initial deposition of the growth strata (**Figure 5**). The sign layer consists of alluvial conglomerate interbedding with sandstone at the top layer of Atushi Formation. The low-angular unconformity starting from the dip angles of the sign layer are abruptly varying from 56° to 45° (**Figures 2C**, **5B**). Meanwhile, the width of the strata under the sign layer is constant (W_4, W_5, and W_6 in **Figure 5C**), but upward of the sign layer, the width of the strata is distinctly becoming thinner toward the crest, indicating that they accumulated during deformation (W_1, W_2, and W_3 in **Figure 5C**).

Timing of Syntectonic Deformation of ATA

The geological age of Pliocene–Pleistocene deposits in the KFTB is still controversial in previous studies (Chen et al., 2002; Sobel et al., 2006; Heermance et al., 2008). By using magnetostratigraphy dating data, Chen et al. (2002) suggested that the boundary ages between the Atushi Formation and Xiyu Conglomerate on the east bank of the Boguzi River and Ganhangou sections are ~1.9 and ~1.0 Ma, respectively. Consequently, they firstly proposed that the initial deformation time of ATA might start at ~1.4 and ~1.2 Ma in the above-mentioned two sections. However, the magnetostratigraphic sampling section located on the east bank of Boguzi River, where a secondary-scale anticline developed, led to the duplication of the Pliocene–Pleistocene strata (**Figures 2**, **4A**). The duplication of sedimentary stratigraphic units might bring confusion to the magnetochronological age data which relies on the continuous deposition of sedimentary strata. Moreover, the fine sandstone and argillite layers suitable for paleomagnetic study are very limited in the boundary between Atushi Formation and Xiyu Conglomerate. Thus, the timing of Xiyu Conglomerate age from a magnetochronological study remains uncertain, and accurate age dating of the growth strata and detailed research of structural deformation are urgently needed to constrain the Pliocene–Pleistocene tectonic deformation of ATA.

In this study, the ^{26}Al/^{10}Be burial age of the growth strata indicates that the initial deformation time of ATA can be traced to 1.79 ± 0.16 Ma, which is almost equal to 1.7 Ma (Sobel et al.,

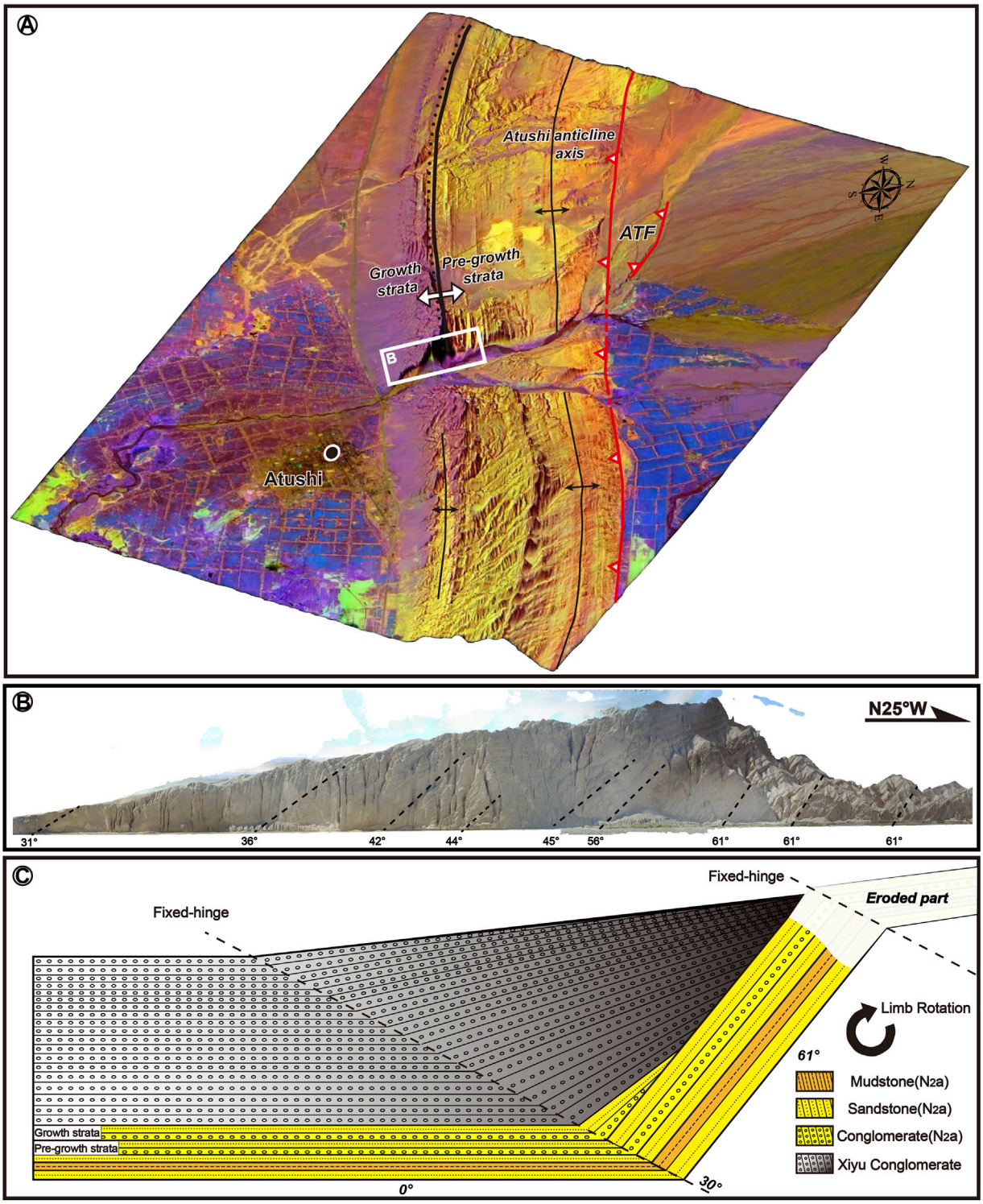

FIGURE 4 | (A) The 3D model of Boguzi River section. **(B)** Spliced pictures of the UAV horizontal imitating ground flight. **(C)** Geometry of the southern limb of Atushi anticline (ATA) and growth mechanism model of ATA based on our field mapping and the cross-section of ATA (Chen et al., 2002; Scharer et al., 2004; Li et al., 2018).

2006) and is different from ~1.4 Ma (Chen et al., 2002). Meanwhile, we proposed that the initial deposit time of Xiyu Conglomerate is about 1.67 ± 0.18 Ma, which is different from ~1.9 Ma in the eastern bank of Boguzi River section and ~1.0 Ma at the Ganhangou section. This phenomenon may be caused by the diachronous deposition of Xiyu Conglomerate (Chen et al.,

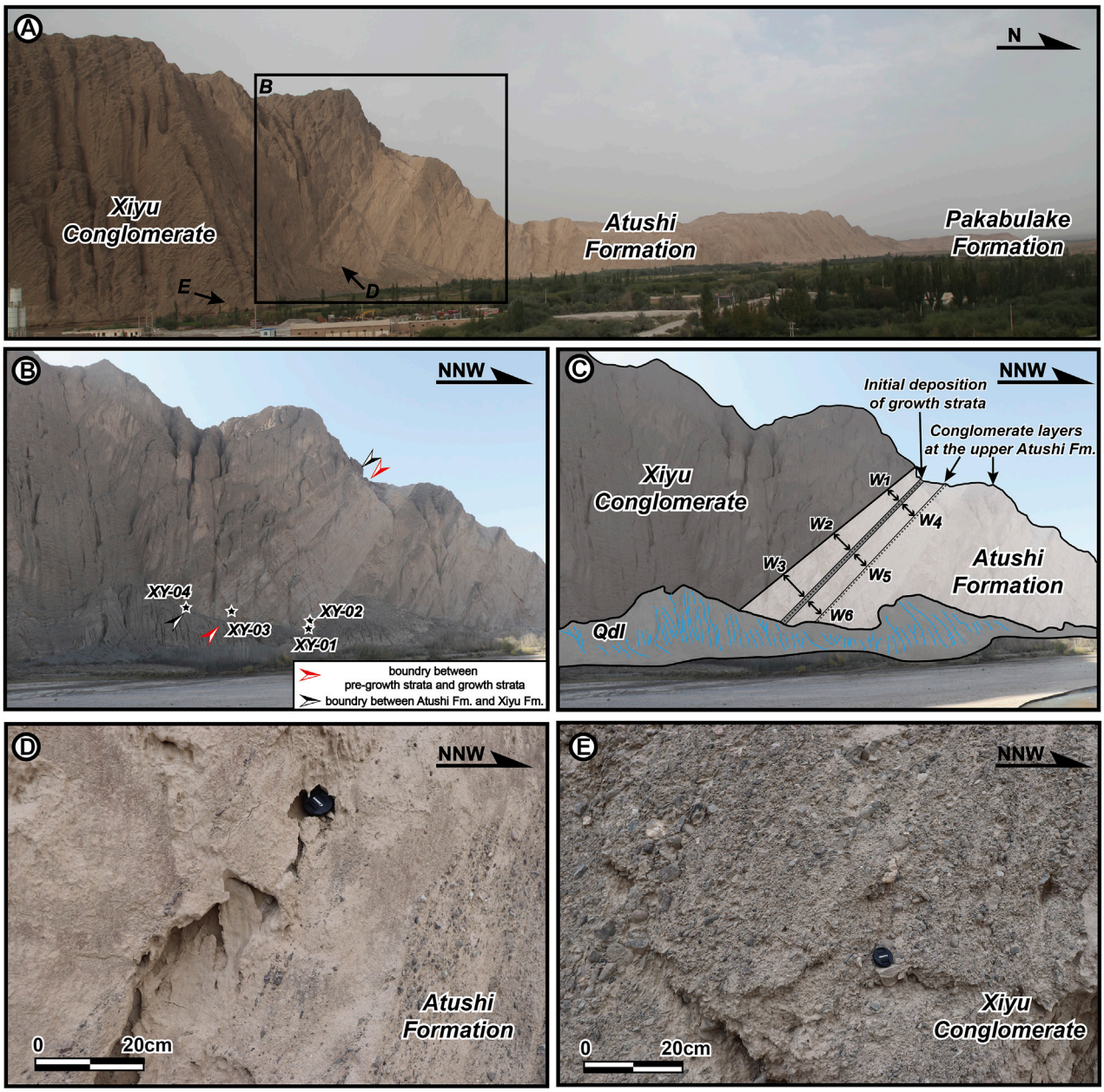

FIGURE 5 | Photographs showing the sedimentary strata near the boundary between Atushi Formation and Xiyu Conglomerate. **(A)** Photograph showing the geological section in the western bank of Boguzi River section. **(B)** Pliocene–Pleistocene strata. The black–white stars show the sampling points of four samples (XY01–XY04). The red arrow means the initial deposition boundary of growth strata and pre-growth strata. The black arrow represents the boundary between Atushi Formation and Xiyu Conglomerate. **(C)** Interpretation of photographs: W_1–W_6 indicated the internal width of adjacent coarse-grained layers, which developed at the top layer of Atushi Formation. **(D)** Photograph showing the sedimentary features of Atushi Fm. **(E)** Photograph showing the sedimentary features of Xiyu Conglomerate.

2000; Chen et al., 2007a; Chen et al., 2007b; Heermance et al., 2007; Qiao et al., 2016). The initial tectonic deformation age of ATA is similar to the middle Kalayuergun anticline (2.6–1.7 Ma) located at the western end of Baicheng-Kuqa foreland fold-and-thrust belt (Lv et al., 2019).

The previous studies have constrained the initial deformation time of west Atushi anticline (ca.3.8 Ma; Thompson-Jobe et al., 2018) and the Ganhangou section of Atushi anticline (1.2 Ma, Chen et al., 2002), respectively. Combined with the initial deformation age of the west bank of the Boguzi River section of Atushi anticline (1.79 Ma in this study), it can be concluded that the ages of the growth strata eastward along the Atushi anticline were younger. Therefore, the fold might have propagated eastward during the Pliocene to Quaternary, and the rate of lateral propagation is 18.6–24.3 km/Ma.

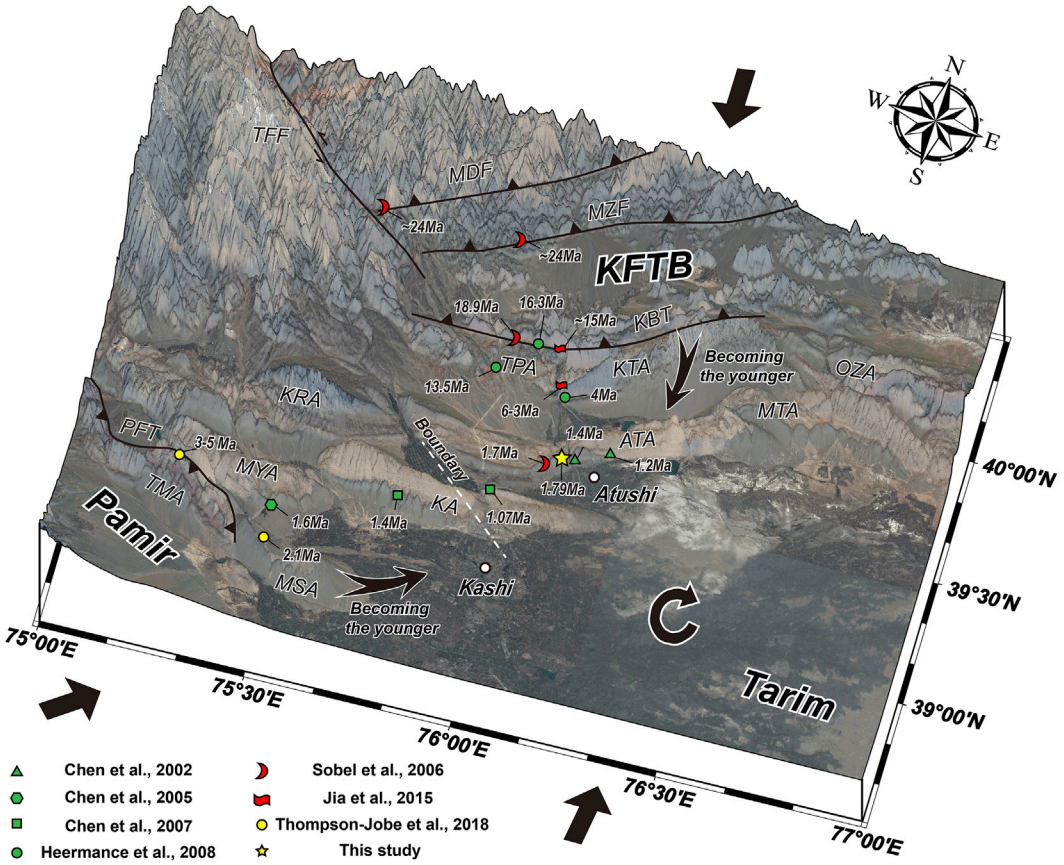

FIGURE 6 | Late Cenozoic deformation age of thrust–fold belts in the Pamir–Tian Shan convergence zone. The initial deformation ages of thrust–fold belts are becoming younger from Muziduke fault to the north flank of Kashi anticline in front of southwestern Tian Shan, displaying a southward propagation process in the Kashi foreland thrust–fold belt. The initial deformation ages of thrust–fold belts in front of northeastern Pamir are also becoming younger, suggesting a northward propagation process in northeastern Pamir.

Figure 6 shows that the initial deformation ages of thrust–fold belts are becoming younger from MZF to the north flank of KA in front of southwestern Tian Shan (Chen et al., 2002; Sobel et al., 2006; Chen et al., 2007a; Heermance et al., 2008; Jia et al., 2015), which indicated the southward multi-stage propagation processes in the KFTB. Meanwhile, recent studies also proposed that the initial deformation ages of the thrust–fold belts in front of northeastern Pamir are also becoming younger, which suggests a northward propagation process in northeastern Pamir (**Figure 6**; Chen et al., 2005, Chen et al., 2007a; Thompson-Jobe et al., 2018). The boundary of two opposite-verging thrust–fold belts along the PTCZ is likely distributed along KA (**Figure 6**; Fu et al., 2010).

CONCLUSION

The tectonic deformation of syntectonic growth strata related to a natural growth fold can provide a key to understand the coupling mechanisms of the sedimentary basin (KFTB) and adjacent southwestern Tian Shan orogenic belt. Our results from the geological and geomorphological interpretations of multiple remote sensing images as well as field investigations conclude that:

(1) The NEE-striking ATA extends about 60 km from the Old Atushi town in the west to the MTA in the east, with a steep limb at the north and a gentle limb at the south. The Miocene Pakabulake Formation is developed in the core, and the Pliocene–Pleistocene Atushi Formation and Xiyu Conglomerate are exposed in the southern limb.

(2) Syntectonic growth strata developed at the southern limb of ATA, which caused the dip angles of Pliocene–Pleistocene strata abruptly changing southward from 56° to 45°, and the width of the strata is distinctly becoming thinner toward the crest at the top part of Atushi Formation. The initial deposit of the growth strata could represent the onset of limb rotation deformation of ATA.

(3) The cosmogenic nuclide $^{26}Al/^{10}Be$ burial age could be constrained as the initial time of growth strata at 1.79 ± 0.16 Ma. The initial deposit of the diachronous Xiyu

Conglomerate began at about 1.67 ± 0.18 Ma. The late Pliocene to early Pleistocene is an important episode of intracontinental deformation in the KFTB, which is a tectonic–sedimentary response to the ongoing convergence between Pamir and Tian Shan.

DATA AVAILABILITY STATEMENT

The original contributions presented in the study are included in the article/Supplementary Material, further inquiries can be directed to the corresponding author.

AUTHOR CONTRIBUTIONS

QC and BF designed the study, did the fieldwork, and wrote the manuscript. PS worked on the processing of UAV remote sensing data and field investigations. PK contributed to age dating of the cosmogenic nuclide samples.

FUNDING

This work was funded by the Strategic Priority Research Program of the Chinese Academy of Sciences (XDA 20070202) and the Second Tibetan Plateau Scientific Expedition and Research Program (STEP, grant no. 2019QZKK0901).

ACKNOWLEDGMENTS

We appreciate the two reviewers for their constructive comments and suggestions, which help to largely improve the quality of this paper. We also gratefully acknowledge the beneficial discussion of Dr. Zhenyu Wang of the Institute of Earthquake Forecasting, China Earthquake Administration.

REFERENCES

Allen, M. B., Vincent, S. J., and Wheeler, P. J. (1999). Late Cenozoic Tectonics of the Kepingtage Thrust Zone: Interactions of the Tien Shan and Tarim Basin, Northwest China. *Tectonics* 18 (4), 639–654. doi:10.1029/1999TC900019

Avouac, J. P., Tapponnier, P., Bai, M., You, H., and Wang, G. (1993). Active Thrusting and Folding along the Northern Tien Shan and Late Cenozoic Rotation of the Tarim Relative to Dzungaria and Kazakhstan. *J. Geophys. Res.* 98, 6755–6804. doi:10.1029/92JB01963

Balco, G., and Shuster, D. L. (2009). ^{26}Al–^{10}Be–^{21}Ne Burial Dating. *Earth Planet. Sci. Lett.* 286 (3-4), 570–575. doi:10.1016/j.epsl.2009.07.025

Burtman, V. S., and Molnar, P. (1993). Geological and Geophysical Evidence for Deep Subduction of Continental Crust beneath the Pamir. *Geol. Soc. America* 281, 1–76. doi:10.1130/SPE281-p1

Chen, J., Ding, G., Burbank, D. W., Scharer, K., Rubin, C., Sobel, E., et al. (2001). Late Cenozoic Tectonics and Seismicity in the Southwestern Tianshan, China. *Earthquake research in China* 17 (2), 134–155. [in Chinese with English abstract]. CNKI:SUN:ZGZD.0.2001-02-003.

Chen, H. L., Chen, Y. G., Chen, S. Q., Lin, X. B., Yang, R., Cheng, X. G., et al. (2019). The Tectonic Processes and Geomorphic Characteristics of Pamir Salient. *Acta Geoscientica Sinica* 40 (1), 55–75. [in Chinese with English abstract]. doi:10.3975/cagsb.2018.092603

Chen, J., Burbank, D. W., Scharer, K. M., Sobel, E., Yin, J. H., Rubin, C., et al. (2002). Magnetochronology of the Upper Cenozoic Strata in the Southwestern Chinese Tian Shan: Rates of Pleistocene Folding and Thrusting. *Earth Planet. Sci. Lett.* 195 (1-2), 113–130. doi:10.1016/S0012-821X(01)00579-9

Chen, J., Heermance, R., Burbank, D. W., Scharer, K. M., Miao, J., and Wang, C. (2007a). Quantification of Growth and Lateral Propagation of the Kashi Anticline, Southwest Chinese Tian Shan. *J. Geophys. Res.* 112 (B3). doi:10.1029/2006jb004345

Chen, J., Heermance, R. V., Burbank, D. W., Scharer, K. M., and Wang, C. S. (2007b). Magnetochronology and its Implications of the Xiyu Conglomerate in the Southwestern Chinese Tian Shan Foreland. *Quat. Sci.* 27 (4), 576–587. [in Chinese with English abstract]. doi:10.3321/j.issn:1001-7410.2007.04.014

Chen, J., Scharer, K. M., Burbank, D. W., Heermance, R. V., and Wang, C. S. (2005). Quaternary Detachment Folding of the Mingyaole Anticline, Southwestern Tian Shan. *Seismology Geology.* 27 (4), 530–547. [in Chinese with English abstract]. doi:10.3969/j.issn.0253-4967.2005.04.002

Chen, J., Yin, J. H., Qu, G. S., and Zhang, K. Q. (2000). Timing, Lower Boundary, Genesis, and Deformation of Xiyu Formation Around the Western Margins of the Tarim basin. *Seismology Geology.* 22, 104–116. [in Chinese with English abstract] CNKI:SUN:DZDZ.0.2000-S1-014. doi:10.3969/j.issn.0253-4967.2005.04.002

Fu, B., Ninomiya, Y., and Guo, J. (2010). Slip Partitioning in the Northeast Pamir-Tian Shan Convergence Zone. *Tectonophysics* 483 (3-4), 344–364. doi:10.1016/j.tecto.2009.11.003

Gao, R., Hou, H., Cai, X., Knapp, J. H., He, R., Liu, J., et al. (2013). Fine Crustal Structure beneath the junction of the Southwest Tian Shan and Tarim Basin, NW China. *Lithosphere* 5 (4), 382–392. doi:10.1130/l248.1

Granger, D. E., Lifton, N. A., and Willenbring, J. K. (2013). A Cosmic Trip: 25 Years of Cosmogenic Nuclides in Geology. *Geol. Soc. America Bull.* 125 (9-10), 1379–1402. doi:10.1130/b30774.1

Granger, D. E., and Muzikar, P. F. (2001). Dating Sediment Burial with In Situ-produced Cosmogenic Nuclides: Theory, Techniques, and Limitations. *Earth Planet. Sci. Lett.* 188, 269–281. doi:10.1016/S0012-821X(01)00309-0

Hardy, S., and Cardozo, N. (2021). Discrete Element Modelling of Sedimentation and Tectonics: Implications for the Growth of Thrust Faults and Thrust Wedges in Space and Time, and the Interpretation of Syn-Tectonic (Growth) Strata. *Front. Earth Sci.* 9. doi:10.3389/feart.2021.742204

Heermance, R. V., Chen, J., Burbank, D. W., and Miao, J. J. (2008). Temporal Constraints and Pulsed Late Cenozoic Deformation during the Structural Disruption of the Active Kashi Foreland, Northwest China. *Tectonics* 27 (6). doi:10.1029/2007tc002226

Heermance, R. V., Chen, J., Burbank, D. W., and Wang, C. (2007). Chronology and Tectonic Controls of Late Tertiary Deposition in the Southwestern Tian Shan Foreland, NW China. *Basin Res.* 19 (4), 599–632. doi:10.1111/j.1365-2117.2007.00339.x

Hubert-Ferrari, A., Suppe, J., Gonzalez-Mieres, R., and Wang, X. (2007). Mechanisms of Active Folding of the Landscape (Southern Tian Shan, China). *J. Geophys. Res.* 112 (B3). doi:10.1029/2006jb004362

Jia, Y., Fu, B., Jolivet, M., and Zheng, S. (2015). Cenozoic Tectono-Geomorphological Growth of the SW Chinese Tian Shan: Insight from AFT and Detrital Zircon U-Pb Data. *J. Asian Earth Sci.* 111, 395–413. doi:10.1016/j.jseaes.2015.06.023

John, H. S., and David, A. M. (1997). Effect of Initial Fault Geometry on the Development of Fixed-Hinge, Fault-Propagation Folds. *J. Struct. Geology.* 19 (12), 1537–1541. doi:10.1016/S0191-8141(97)00065-5

Jungers, M. C., and Heimsath, A. M. (2015). Post-tectonic Landscape Evolution of a Coupled basin and Range: Pinaleño Mountains and Safford Basin, southeastern Arizona. *Geol. Soc. America Bull.* 128 (3-4), 469–486. doi:10.1130/b31276.1

Kong, P., Zheng, Y., and Fu, B. (2011). Cosmogenic Nuclide Burial Ages and Provenance of Late Cenozoic Deposits in the Sichuan Basin: Implications for Early Quaternary Glaciations in East Tibet. *Quat. Geochronol.* 6 (3-4), 304–312. doi:10.1016/j.quageo.2011.03.006

Korschinek, G., Bergmaier, A., Faestermann, T., Gerstmann, U. C., Knie, K., Rugel, G., et al. (2010). A New Value for the Half-Life of 10Be by Heavy-Ion Elastic

Recoil Detection and Liquid Scintillation Counting. *Nucl. Instr. Methods Phys. Res. Section B: Beam Interactions Mater. Atoms* 268 (2), 187–191. doi:10.1016/j.nimb.2009.09.020

Lal, D., and Arnold, J. R. (1985). Tracing Quartz through the Environment. *J. Earth Syst. Sci.* 94 (1), 1–5. doi:10.1007/bf02863403

Li, T., Chen, J., Thompson, J. A., Burbank, D. W., and Yang, H. (2015). Hinge-migrated Fold-scarp Model Based on an Analysis of Bed Geometry: A Study from the Mingyaole Anticline, Southern Foreland of Chinese Tian Shan. *J. Geophys. Res. Solid Earth* 120 (9), 6592–6613. doi:10.1002/2015jb012102

Li, T., Chen, J., Thompson, J. A., Burbank, D. W., and Yang, X. (2013). Quantification of Three-Dimensional Folding Using Fluvial Terraces: A Case Study from the Mushi Anticline, Northern Margin of the Chinese Pamir. *J. Geophys. Res. Solid Earth* 118 (8), 4628–4647. doi:10.1002/jgrb.50316

Li, T., Chen, J., Thompson Jobe, J. A., Burbank, D. W., Cheng, X., Xu, J., et al. (2018). Active Bending-Moment Faulting: Geomorphic Expression, Controlling Conditions, Accommodation of Fold Deformation. *Tectonics* 37, 2278–2306. doi:10.1029/2018TC004982

Li, Z., Li, T., Almeida, R., Zhang, P., Zheng, W., Sun, C., et al. (2019). Lateral Fault Growth in the Kashi Anticline (Chinese Tian Shan): Insights from Seismic Interpretation, Shortening Distribution, and Trishear Methods. *J. Geophys. Res. Solid Earth* 124 (7), 7303–7319. doi:10.1029/2018jb017186

Liu, T. S., Ding, M. L., and Edward, D. (1996). Gravel Deposits on the Margins of the Qinghai-Xizang Plateau, and Their Environmental Significance. *Palaeogeogr. Palaeoclimatol. Palaeoecol.* 120 (1-2), 159–170. doi:10.1016/0031-0182(95)00039-9

Lü, L., Sun, J., Zhang, Z., Jia, Y., Li, T., Li, C., et al. (2019). Cenozoic Deformation and Crustal Shortening in the Foreland of Southern Tian Shan, NW China, as a Response to the India-Asia Collision. *J. Asian Earth Sci.* 183, 103960. doi:10.1016/j.jseaes.2019.103960

McCalpin, J. P., and Nelson, A. R. (1996). Chapter 1 Introduction to Paleoseismology. *Int. Geophys.* 62, 1–32. doi:10.1016/s0074-6142(96)80068-4

Molnar, P., and Tapponnier, P. (1975). Cenozoic Tectonics of Asia: Effects of a Continental Collision: Features of Recent continental Tectonics in Asia Can Be Interpreted as Results of the India-Eurasia Collision. *Science* 189 (4201), 419–426. doi:10.1126/science.189.4201.419

Poblet, J., McClay, K., Storti, F., and Mufioz, J. A. (1997). Geometries of Syntectonic Sediments Associated with Single-Layer Detachment Folds. *J. Struct. Geology.* 19 (3), 369–381. doi:10.1016/S0191-8141(96)00113-7

Qiao, Q., Huang, B., Piper, J. D. A., Deng, T., and Liu, C. (2016). Neogene Magnetostratigraphy and Rock Magnetic Study of the Kashi Depression, NW China: Implications to Neotectonics in the SW Tianshan Mountains. *J. Geophys. Res. Solid Earth* 121 (3), 1280–1296. doi:10.1002/2015jb012687

Qu, G., Chen, J., Chen, X., Canerot, J., and Li, Y. (2001). A Study on the Back-Thrusting System at Atushi-Bapanshuimo in Tarim Basin. *Seismology and Geology* 23, 1–14. [in Chinese with English abstract].

Riba, O. (1976). Syntectonic Unconformities of the Alto Cardener, Spanish Pyrenees: a Genetic Interpretation. *Sediment. Geology.* 15, 213–233. doi:10.1016/0037-0738(76)90017-8

Salvini, F., and Storti, F. (2002). Three-dimensional Architecture of Growth Strata Associated to fault-bend, Fault-Propagation, and Décollement Anticlines in Non-erosional Environments. *Sediment. Geology.* 146, 57–73. doi:10.1016/S0037-0738(01)00166-X

Scharer, K. M., Burbank, D. W., Chen, J., Weldon, R. J., Rubin, C., Zhao, R., et al. (2004). Detachment Folding in the Southwestern Tian Shan-Tarim Foreland, China: Shortening Estimates and Rates. *J. Struct. Geology.* 26, 2119–2137. doi:10.1016/j.jsg.2004.02.016

Shaw, J. H., and Suppe, J. (1994). Active Faulting and Growth Folding in the Eastern Santa Barbara Channel, California. *Geol. Soc. America Bull.* 106 (5), 607–626. doi:10.1130/0016-7606(1994)106<0607:afagfi>2.3.co;2

Sobel, E., Chen, J., and Heermance, R. (2006). Late Oligocene-Early Miocene Initiation of Shortening in the Southwestern Chinese Tian Shan: Implications for Neogene Shortening Rate Variations. *Earth Planet. Sci. Lett.* 247 (1-2), 70–81. doi:10.1016/j.epsl.2006.03.048

Sobel, E. R., and Dumitru, T. A. (1997). Thrusting and Exhumation Around the Margins of the Western Tarim basin during the India-Asia Collision. *J. Geophys. Res.* 102 (B3), 5043–5063. doi:10.1029/96jb03267

Sun, J., Li, Y., Zhang, Z., and Fu, B. (2009). Magnetostratigraphic Data on Neogene Growth Folding in the Foreland basin of the Southern Tianshan Mountains. *Geology* 37 (11), 1051–1054. doi:10.1130/g30278a.1

Sun, J. M., Zhu, R. X., and Bowler, J. (2004). Timing of the Tianshan Mountains Uplift Constrained by Magnetostratigraphic Analysis of Molasse Deposits. *Earth Planet. Sci. Lett.* 219 (3-4), 239–253. doi:10.1016/s0012-821x(04)00008-1

Sun, J., and Zhang, Z. (2009). Syntectonic Growth Strata and Implications for Late Cenozoic Tectonic Uplift in the Northern Tian Shan, China. *Tectonophysics* 463 (1-4), 60–68. doi:10.1016/j.tecto.2008.09.008

Suppe, J., Chou, G. T., and Hook, S. C. (1992). Rates of Folding and Faulting Determined from Growth Strata. *Thrust Tectonics*, 105–121. doi:10.1007/978-94-011-3066-0_9

Thompson-Jobe, J. A., Burbank, D. W., Li, T., Chen, J., and Bookhagen, B. (2015). Late Miocene Northward Propagation of the Northeast Pamir Thrust System, Northwest China. *Tectonics* 34 (3), 510–534. doi:10.1002/2014tc003690

Thompson-Jobe, J. A., Li, T., Bookhagen, B., Chen, J., and Burbank, D. (2018). Dating Growth Strata and basin Fill by Combining 26Al/10Be Burial Dating and Magnetostratigraphy: Constraining Active Deformation in the Pamir-Tian Shan Convergence Zone, NW China. *Lithosphere* 10 (6), 806–828. doi:10.1130/L727.1

Thompson-Jobe, J. A., Li, T., Chen, J., Burbank, D. W., and Bufe, A. (2017). Quaternary Tectonic Evolution of the Pamir-Tian Shan Convergence Zone, Northwest China. *Tectonics* 36 (12), 2748–2776. doi:10.1002/2017tc004541

Tian, Q., Ding, G., Hao, P., Canerot, J., and Li, Y. (2006). Seismotectonic Study on West Part of the Interaction Zone Between Southern Tianshan and Northern Tarim. *Seismology and Geology* 28, 213–223. [in Chinese with English abstract].

Wu, C., Zheng, W., Zhang, P., Zhang, Z., Jia, Q., Yu, J., et al. (2019). Oblique Thrust of the Maidan Fault and Late Quaternary Tectonic Deformation in the Southwestern Tian Shan, Northwestern China. *Tectonics* 38 (8), 2625–2645. doi:10.1029/2018tc005248

Yang, X., Chen, L., Li, A., Du, L., and Deng, Q. (2009). Late Quaternary Phased Uplift of the Atushi Anticline in the Southwestern Tianshan. *Earth Science Frontiers* 16 (3), 160–170. [in Chinese with English abstract] CNKI:SUN:DXQY.0.2009-03-018.

Yin, A., Nie, S., Craig, P., Harrison, T. M., Ryerson, F. J., Xianglin, Q., et al. (1998). Late Cenozoic Tectonic Evolution of the Southern Chinese Tian Shan. *Tectonics* 17 (1), 1–27. doi:10.1029/97tc03140

Zhang, Z., Han, W., Fang, X., Song, C., and Li, X. (2013). Late Miocene-Pleistocene Aridification of Asian Inland Revealed by Geochemical Records of Lacustrine-Fan delta Sediments from the Western Tarim Basin, NW China. *Palaeogeogr. Palaeoclimatol. Palaeoecol.* 377, 52–61. doi:10.1016/j.palaeo.2013.03.008

Zhao, R. B., Li, J., and Shen, J. (2001). Preliminary Study on the Deformation Features and Seismogenic Model of the 1902 Artux, Xinjiang Earthquake of Ms8¼. *Seismology Geology.* 23 (4), 581–587. [in Chinese with English abstract]. doi:10.1007/s11769-000-0051-4

Conflict of Interest: The authors declare that the research was conducted in the absence of any commercial or financial relationships that could be construed as a potential conflict of interest.

Publisher's Note: All claims expressed in this article are solely those of the authors and do not necessarily represent those of their affiliated organizations, or those of the publisher, the editors and the reviewers. Any product that may be evaluated in this article, or claim that may be made by its manufacturer, is not guaranteed or endorsed by the publisher.